ehp ENVIRONMENTAL HEALTH PERSPECTIVES
http://www.ehponline.org

Ligand Binding and Activation of PPARγ by Firemaster® 550: Effects on Adipogenesis and Osteogenesis *in Vitro*

Hari K. Pillai, Mingliang Fang, Dmitri Beglov, Dima Kozakov, Sandor Vajda, Heather M. Stapleton, Thomas F. Webster, and Jennifer J. Schlezinger

http://dx.doi.org/10.1289/ehp.1408111
Received: 10 January 2014
Accepted: 24 July 2014
Advance Publication: 25 July 2014

NIH National Institute of Environmental Health Sciences

Ligand Binding and Activation of PPARγ by Firemaster® 550: Effects on Adipogenesis and Osteogenesis *in Vitro*

Hari K. Pillai,[1] Mingliang Fang,[2] Dmitri Beglov,[3] Dima Kozakov,[3] Sandor Vajda,[3] Heather M. Stapleton,[2] Thomas F. Webster,[1] and Jennifer J. Schlezinger[1]

[1]Department of Environmental Health, Boston University, Boston, Massachusetts, USA;

[2]Nicholas School of the Environment, Duke University, Durham, North Carolina, USA;

[3]Department of Biomedical Engineering, Boston University, Boston, Massachusetts, USA

Address correspondence to Jennifer J. Schlezinger, Boston University School of Public Health, Dept. of Environmental Health, 715 Albany Street, R-405, Boston, MA 02118 USA. Telephone: 617-638-6497. E-mail: jschlezi@bu.edu

Running title: PPARγ activation by an alternative flame retardant

Acknowledgments: The authors would like to thank Ms. Faye Andrews for her superb technical assistance. Analytical assistance was provided by the Bioinformatics and Molecular Modeling Core of the Boston University Superfund Program. This work was supported by Superfund Research Program grants P42ES007381 (J.J.S, T.F.W, H.P., D.B., D.K., S.V.) and P42ES010356 (H.M.S., M.F.), R01ES015829 (T.F.W.) and R01ES016099 (H.M.S., M.F.) from the National Institute of Environmental Health Science and R01GM064700 (D.B., D.K., SV) from the National Institute of General Medical Sciences.

Competing financial interests: The authors declare they have no actual or potential competing financial interests.

Abstract

Background: Alternative flame retardant use has increased since the phase out of pentabromodiphenyl ethers. One alternative, Firemaster® 550 (FM550), induces obesity in rats. Triphenyl phosphate (TPP), a component of FM550, has a structure similar to organotins, which are obesogenic in rodents.

Objectives: We tested the hypothesis that FM550 components are biologically active peroxisome proliferator activated receptor γ (PPARγ) ligands and estimated indoor exposure to TPP.

Methods: FM550 and its components were assessed for ligand binding to and activation of human PPARγ. Solvent mapping was used to model TPP in the PPARγ binding site. Adipocyte and osteoblast differentiation were assessed in bone marrow multipotent mesenchymal stromal cell models. We estimated exposure of children to TPP using house dust concentrations determined in a previously published study and a screening-level indoor exposure model.

Results: FM550 bound human PPARγ and binding appeared to be driven primarily by TPP. Solvent mapping revealed that TPP interacts with binding hotspots within the PPARγ ligand binding domain. FM550 and its organophosphate components increased human PPARγ1 transcriptional activity in a Cos7 reporter assay and induced lipid accumulation and perilipin protein expression in BMS2 cells. FM550 and TPP diverted osteogenic differentiation toward adipogenesis in primary mouse bone marrow cultures. Our estimates suggest that dust ingestion is the major route of exposure of children to TPP.

Conclusions: Our findings suggest that FM550 components bind and activate PPARγ. In addition, *in vitro* exposure initiated adipocyte differentiation and antagonized osteogenesis. TPP likely is a major contributor to these biological actions. Given that TPP is ubiquitous in house dust, further studies are warranted to investigate health effects of FM550.

Introduction

Flammability standards, such as California's Technical Bulletin 117 (BHFTI 2000), led to addition of flame retardants at percent levels in residential furniture, making these chemicals a ubiquitous component of the human indoor environment. The US production phase-out of commercial pentabromodiphenyl ethers (PentaBDE) in 2004 led to an increased demand for alternatives such as organophosphate flame retardants (OPFRs) and a commercial mixture known as Firemaster® 550 (FM550). FM550 is composed of bis-(2-ethylhexyl) tetrabromophthalate (TBPH), a brominated analogue of bis-(2-ethylhexyl) phthalate that is a known obesogen (Feige et al. 2010), tetrabromobenzoate (TBB), and a mixture of triaryl phosphates including triphenyl phosphate (TPP) and several isomers of mono-, di- and tri-isopropylated triaryl phosphates (ITP). The brominated and organophosphate components each comprise approximately 50% of FM550 (Stapleton et al. 2008). High levels of OPFRs have been found in dust collected from homes, offices and cars, with concentrations of TPP alone as high as 1.8 mg/g in house dust (Carignan et al. 2013; Meeker et al. 2013; Stapleton et al. 2009). OPFR metabolites are ubiquitous in human urine (Carignan et al. 2013; Cooper et al. 2011; Meeker et al. 2013).

Pre- and postnatal exposure to FM550 resulted in increased anxiety, obesity, and early puberty in rats, with the non-behavioral effects occurring at a dose of 1 mg per pregnant rat per day or approximately 2.5 mg FM550/kg/day (Patisaul et al. 2013). As TPP represents between 10-20% of the FM550 mixture, this equates to approximately 250 µg TPP/kg/day. These data suggest that a component, or components, of FM550 is acting as an environmental obesogen, a chemical that disrupts the homeostatic controls of adipogenesis and energy balance (Grun et al. 2006). Similarly, increased adiposity has been observed in rodents exposed to tributyltin and phthalates

(Feige et al. 2010; Grun et al. 2006). These obesogens are agonists of peroxisome proliferator activated receptor γ (PPARγ) (Feige et al. 2007; Grun et al. 2006), a nuclear receptor and master regulator of adipogenesis (Tontonoz and Spiegelman 2008). Interestingly, TPP has been shown to interact with a variety of nuclear receptors, activating constitutive androstane receptor, pregnane X receptor, and estrogen receptor-mediated reporter activity and antagonizing androgen, progesterone, and glucocorticoid receptor-mediated reporter activity (Honkakoski et al. 2004; Kojima et al. 2013; Suzuki et al. 2013). TPP's ability to interact with PPARγ remains to be elucidated.

Based on the profound adiposity induced by FM550 *in vivo* and evidence that OPFRs can act as nuclear receptor ligands, the studies described herein were designed to test the hypothesis that components of FM550 are biologically active PPARγ ligands. Accordingly, we examined FM550, as well as the components TPP and ITP, for the ability to bind PPARγ, to initiate PPARγ-dependent transcription, to induce mature adipocyte differentiation, and to divert bone marrow multipotent mesenchymal stromal cell (MSC) differentiation away from osteogenesis. We also estimated the potential contribution of dust ingestion to TPP exposure based on previous measurements in dust and a screening-level exposure model for semivolatile organic compounds (SVOCs). Overall, the data presented here are consistent with FM550 containing a PPARγ ligand and with TPP being a major contributor to PPARγ activation. TPP not only induced adipocyte differentiation but also antagonized osteogenesis in primary mouse bone marrow cultures.

Materials and Methods

Materials

Human insulin, Nile Red, tributyltin chloride (96%) and TPP (≥99%) were from Sigma-Aldrich (St. Louis, MO). A commercial mixture of ITP was purchased from the Chinese manufacturer

Jinan Great Chemical Industry Co., Ltd (Commercial Grade, Jinan, PRC). FM550 was provided as a gift to Dr. Susan Klosterhaus (Stapleton et al. 2008) from Chemtura Inc. TBPH (99.5% by GC/MS) and TBB (97.3% by GC/MS) were from Accustandard (New Haven, CT). All other reagents were from Thermo Fisher Scientific (Suwanee, GA), unless noted.

Dose solution preparation and estimation of mixture molar concentrations

Dose solutions were prepared based on weight per volume for FM550 and ITP. Dose solutions were prepared on a molar basis for TPP, TBB, TBPH and rosiglitazone. All dose solutions were prepared in DMSO. Molecular weights for the FM550 and ITP mixtures were estimated based on the molecular weights of individual components and their typical percentages in these mixtures (see Supplemental Material, Table S1). Molar concentrations in the experiments were then estimated using the calculated molecular weights (see Supplemental Material, Table S2). For FM550 and ITP, the concentrations are reported as weight per volume, followed by the estimate of the molar concentration.

PPARγ ligand binding assay

Human PPARγ binding was quantified using the PolarScreen™ PPARγ-Competitor Assay Kit (Invitrogen, Carlsbad, CA), according to the manufacturer's instructions. In brief, human recombinant PPARγ ligand-binding domain (LBD)-GST and Fluoromone™ PPARγ Green, a tight-binding, selective fluorescent PPARγ ligand, were mixed with test compounds. FM550 (0.01-70 μg/ml; 0.02-160 μM), TPP (0.01-1400 μM), TBB (0.009-90 μM), TBPH (0.12-1200 μM), ITP (0.01-28 μg/ml; 0.02-80 μM) and the positive control rosiglitazone (0.00012-12 μM) were prepared in DMSO. Displacement of the fluorescent ligand, which has high polarization when bound to the PPARγ-LBD and low polarization when not bound, was assessed by

measuring loss of fluorescence polarization using a SpectraMax M5 plate reader (Molecular Devices, Sunnyvale, CA). IC_{50} and dissociation constants were calculated to compare the potency of the binding. The latter was calculated according to the following equation:

$$IC_{50}/[\text{PPAR}\gamma\ \text{Green}] = K_{d,ligand}/K_{d,probe} \quad [1]$$

where $K_{d,probe}$ is the dissociation constant calculated from titration of 1.25 nM Fluoromone™ PPARγ Green with the PPARγ-LBD.

Computational analysis of ligand binding to PPARγ

Binding hot spots in the PPARγ LBD were determined using the computational solvent mapping algorithm FTMap (Brenke et al. 2009). The docking of ligands was carried out using the docking program AutoDock Vina 1.1.0 (Trott and Olson 2010). The 10 lowest energy binding poses were retained for each ligand. The selection of the most likely pose was based on the atom densities calculated from the mapping results. We considered each retained ligand pose separately and summed the atomic densities for all heavy atoms, resulting in a measure of overlap between the pose and the probe density. The poses were ranked on the basis of this overlap measure, and the pose with the best overlap was selected as the most likely binding mode (Kozakov et al. 2011) (see Supplemental Material, "Computational Analysis of Ligand Binding to PPARγ," pg. 2, for a detailed description of this analysis).

Reporter assays

Cos-7 cells were transiently transfected with vectors containing human *PPARG1* (provided by V.K. Chatterjee, U. Cambridge) (Gurnell et al. 2000) and human *RXRA* (plasmid 8882; Addgene) (Tontonoz et al. 1994), with PPRE x3-TK-luc (plasmid 1015; Addgene) (Kim et al. 1998) and CMV-eGFP reporter constructs using Lipofectamine2000 (Invitrogen). Cultures were

cotransfected with either pcDNA3 (Invitrogen, Carlsbad, CA) or dominant negative human *PPARG* (PPARγ-DN) (provided by V.K. Chatterjee). Following an overnight incubation, the medium was replaced, and cultures received no treatment (Naïve) or were treated with Vh (DMSO, 0.1%), FM550 (0.1-20 μg/ml; 0.2-50 μM), TPP (0.1-40 μM), ITP (0.1-10 μg/ml; 0.3-60 μM) or rosiglitazone (0.0001-1 μM) and incubated for 24 hrs. Cells were lysed in Glo Lysis Buffer and mixed with Bright Glo reagent (Promega, Madison, WI). Luminescence and fluorescence were determined using a Synergy2 plate reader (Biotek, Inc., Winooski, VT). Luminescence was normalized by the GFP fluorescence in the same well. The normalized luminescence for each well was then divided by the normalized luminescence measured in control, DN-PPARγ-transfected wells to determine the "Fold-Change from DN-Control."

Cell culture

BMS2 cells are C57BL/6 mouse-derived bone marrow stromal cells (Pietrangeli et al. 1988)(provided by P. Kincade, Oklahoma Medical Research Foundation). BMS2 cells were maintained in DMEM with 5% FBS (Sigma-Aldrich), 5 μg/ml plasmocin (Invivogen, San Diego, CA) and 20 mM L-glutamine. Cultures were maintained at 37º C in a humidified, 5% CO_2 atmosphere. BMS2 were plated at 40,000 cells/well (24-well plates) or 160,000 cells/well (6-well plates) in pre-adipocyte medium (DMEM containing 10% FBS, 1mM sodium pyruvate, 100 U/ml penicillin, 100 μg/ml streptomycin) and allowed to become confluent (3-4 days). Prior to dosing, the medium was replaced with pre-adipocyte medium supplemented with insulin (0.5 μg/ml). Cultures received no treatment (Naïve) or were treated with Vh (DMSO, 0.1%), FM550 (0.1 – 10 μg/ml; 0.2-20 μM), ITP (0.1 – 10 μg/ml; 0.3-30 μM), TPP (0.1 – 20 μM) or rosiglitazone (0.001-1 μM). Medium was changed, and the cultures were redosed once. The total exposure period was 7 days.

Primary bone marrow cultures were prepared from C57BL/6J mice (female, 12 weeks of age, Jackson Laboratories, Bar Harbor, ME). Studies were reviewed and approved by the Institutional Animal Care and Use Committee at Boston University. All animals were treated humanely and with regard for alleviation of suffering. Mice were housed 4 per cage, with a 12 hour light cycle. Water and food (2018 Teklad Global 18% Protein Rodent Diet, Irradiated, Harlan Laboratories, Indianapolis, IN) were provided *ad libitum*. Animals were euthanized for collection of bone marrow two days after arrival. After euthanasia, limbs were aseptically dissected, and soft tissue was removed from the bone. Bone marrow was flushed from the femur, tibia and humerus bones using a 25 gauge needle and RPMI media containing 10% FBS, 100 U/ml penicillin, 100 μg/ml streptomycin, and 0.25 μg/ml amphotericin B, strained through a 70 μm cell strainer, diluted in MSC media (α-MEM containing 10% FBS and 100 U/ml penicillin, 100 μg/ml streptomycin, 0.25 μg/ml amphotericin B), and seeded at $6x10^6$/ml in 1 ml per well in a 12-well plate or 2 ml per well in a 6-well plate. Half of the medium was replaced 4 days after plating, and the cultures continued for 3 more days. To induce osteogenesis, the medium was replaced with MSC media supplemented with ascorbate (12.5 μg/ml), β-glycerol phosphate (8 μM), dexamethasone (10 nM), and insulin (500 ng/ml). Cultures received no treatment (Naïve) or were treated with Vh (DMSO, 0.1%), FM550 (0.1-10 μg/ml; 2-20 μM), TPP (0.1-10 μM), or rosiglitazone (0.1 μM). Medium was changed, and the cultures were redosed 3 times for a total exposure period of 7 days (gene expression) or 4 times for a total exposure period of 12-13 days (phenotype).

Cell viability assays

Confluent BMS2 cultures were treated with Vh (DMSO, 0.1%), FM550 (0.1-40 μg/ml; 0.2-90 μM), TPP (0.1-40 μM), ITP (0.1-40 μg/ml; 0.3-100 μM), or rosiglitazone (0.001-1 μM) for 24 hrs, 7 days or 12 days. Treatment with high dose tributyltin (1-4 μM) for 2-3 hrs was used as a

positive control. Medium was changed, and the cultures were redosed as described under Cell Culture. Cellularity was assessed by 3-[4,5-dimethylthiazol-2-yl]-2,5-diphenyltetrazolium bromide (MTT) labeling for 3 hrs by standard methods. Apoptosis and necrosis were assessed by caspase-3 activity (Caspase-Glo® 3/7 Assay, Promega) and dead cell protease release (CytoTox-Glo™ Cytotoxicity Assay, Promega), respectively, according to the manufacturer's instructions. Absorbance and luminescence measurements were determined using a Synergy2 plate reader. Absorbance or luminescence in experimental wells was normalized by dividing by the absorbance or luminescence in untreated cultures and reported as "Fold Change from Medium."

Adipogenesis and osteogenesis assays

First, lipid accumulation was quantified by Nile Red staining (Yanik et al. 2011). The fluorescence in all experimental wells was normalized by subtracting the fluorescence measured in untreated cultures and reported as "Naïve Corrected RFUs." Second, cultures were fixed in 2% paraformaldehyde. To quantify alkaline phosphatase activity, cells were incubated with p-nitrophenyl phosphate solution (Sigma-Aldrich). After quenching with sodium hydroxide, absorbance (405 nM) was measured. Third, cells were stained with Alizarin Red (Osteogenesis Quantitation Kit, Millipore, Billerica, MA), and staining was quantified according to the manufacturer's instructions. For osteogenesis assays, absorbance in experimental wells was normalized by dividing by the absorbance measured in untreated, osteogenic cultures and reported as "Fold Change from Medium." All absorbance and fluorescence measurements were determined using a Synergy2 plate reader.

Immunoblotting

Cells were lysed in Cell Lysis Buffer (Cell Signaling Technology) followed by sonication. Whole cell lysates were used for protein expression analyses. Protein concentrations were

determined by the Bradford method (Bradford 1976). Total proteins (40 μg) were resolved on 10% gels, transferred to a 0.2 μm nitrocellulose membrane, and incubated with monoclonal rabbit anti-perilipin (9349, Cell Signaling Technology (Beverly, MA)). Immunoreactive bands were detected using HRP-conjugated secondary antibodies (Biorad, Hercules, CA) followed by enhanced chemiluminescence. To control for equal protein loading, blots were re-probed with a β-actin-specific antibody (A5441, Sigma-Aldrich) and analyzed as above.

mRNA expression

Total RNA was extracted, and genomic DNA was removed using the RNeasy Plus Mini Kit (Qiagen, Valencia, CA). cDNA was prepared from total RNA using the GoScript™ Reverse Transcription System (Promega). All qPCR reactions were performed using the GoTaq® qPCR Master Mix System (Promega). Validated primers (18s ribosomal RNA (*Rn18s)*: QT01036875, fatty acid binding protein 4 (*Fabp4)*: QT00091532, Sp7 transcription factor 7; Osterix (*Sp7*): QT00293181) were purchased from Qiagen. qPCR reactions were performed using a 7500 Fast Real-Time PCR System (Applied Biosystems, Carlsbad, CA). Relative gene expression was determined using the Pfaffl method (Pfaffl 2001), using the threshold value for *Rn18s* for normalization. No significant differences were observed in the expression of *Rn18s* across the different treatments (data not shown). The Cq value from naïve, undifferentiated cultures prepared from 9-week-old male mice was used as the reference point. Data were reported as "Fold Difference from Naive."

Exposure assessment

We used previously reported TPP dust concentrations from the largest published sample to date: 50 homes sampled in the Boston USA area between 2002-7 using vacuum cleaner bags (Stapleton et al. 2009), which are similar to the few previously reported dust concentrations

(Dodson et al. 2012; Van den Eede et al. 2011). As TPP is an SVOC (Weschler and Nazaroff 2008), the SVOC model of Little et al. (Little et al. 2012) was used to assess indoor exposure to TPP. It estimates exposure via several routes of exposure assuming steady-state conditions: inhalation (vapor and particle bound), dermal absorption of compounds from vapor, and incidental dust ingestion. Dermal absorption from contact with dust or surface films is not included in the model of Little et al (2012), a potentially important limitation. The factor driving the model is y_0, the vapor phase concentration of the SVOC in equilibrium with the material phase concentration compound (C_0) in the product. While we have previously measured C_0 for TPP in furniture foam (Stapleton et al. 2012), there is no generally accepted way to estimate y_0 from C_0 for SVOCs (Little et al. 2012). However, y_0 can be back-calculated from the measured bulk air concentration y (Little et al. 2012) or, as we did, from dust concentrations (C_{dust}) as all three are related in the steady-state model:

$$y_0 = y[1 + (Q^*/hA)] \quad [2]$$

$$y = C_{dust} / K_{dust} \quad [3]$$

where h is the convective mass transfer coefficient over the emission surface, A is the surface area of the source (assumed to be polyurethane foam with an additive flame retardant), Q^* is the equivalent ventilation rate adjusted for particulate-bound SVOCs, and K_{dust} is the dust/vapor partition coefficient (Little et al. 2012). These and other parameters were either taken directly from Little et al. or calculated using the physical-chemical properties of TPP. To facilitate comparisons with other compounds analyzed using this model, we estimated the physical-chemical properties of TPP using SPARC (ARChem 2013): log(K_{OA}) of 10.3 at 25 C, log(K_{OW}) of 7.3 at 32 C, log(K_{WA}) of 2.8 at 32 C. Given the estimate of y_0, the model of Little et al

(2012)—implemented in a spreadsheet provided with their publication—estimates partitioning within a room. Using standard exposure factors, it then provides estimates of exposure via inhalation (vapor and particle bound), dermal absorption of compounds from vapor, and incidental dust ingestion.

Statistics

Statistical analyses and curve fitting were performed with Prism 5 (Graphpad Inc., La Jolla, CA). Data are presented as means ± standard error (SE). The number of replicates is indicated in each figure legend. Gene expression data were log transformed prior to analysis. Dose response curves were fit with the sigmoid 4-parameter Hill function. Data were analyzed for statistical significance using a One-Factor ANOVA, in conjunction with the Dunnett's multiple comparisons test; $p \leq 0.05$ was considered statistically significant.

Results

Analysis of toxicity of FM550 and its organophosphate components

We used the BMS2 bone marrow stromal cell line to assess the toxicity of FM550, TPP and ITP under short and long term dosing regimens. Confluent BMS2 cultures showed no loss of cellularity after treatment for 24 hrs with concentrations as high as 40 μg/ml (90 μM) FM550, 40 μM TPP, or 40 μg/ml (100 μM) ITP or after treatment for 7 days with concentrations as high as 20 μg/ml (50 μM) FM550, 20 μM TPP, or 10 μg/ml (30 μM) ITP (see Supplemental Material, Figure 1SA-B). Confluent BMS2 cultures showed no loss of cellularity, no increase in caspase-3 activity and no increase in necrotic protein release after treatment for 12 days with concentrations as high as 10 μg/ml (20 μM) FM550 or 20 μM TPP (see Supplemental Material, Figure S1C-E). The positive control, tributyltin, showed a significant reduction in cellularity and

significant increases in apoptosis and necrosis, confirming that the assays were functional (see Supplemental Material, Figure S1A-E). Rosiglitazone showed no loss of cellularity following any treatment period up to 12 days at a concentration as high as 1μM (see Supplemental Material, Figure S1A-C).

Assessment of PPARγ activation by FM550

To test the hypothesis that FM550 can activate PPARγ transcriptional activity and directly induce adipogenesis, we began by investigating the ability of FM550 to activate PPARγ-driven reporter activity. Cos7 cells were transfected with human *PPARG1* and *RXRA* expression vectors and a PPRE-driven reporter construct and treated with Vh or FM550. FM550 significantly induced PPARγ-driven reporter activity at concentrations ≥10 μg/ml (20 μM), with an EC_{50} of 47 μM (Figure 1A). The maximal FM550-induced activity of 5.7±0.3-fold was less than the activity induced by a maximally efficacious concentration of rosiglitazone (1 μM; 11.3±0.9-fold; EC_{50} of 0.02 μM; see Supplemental Material, Figure S2A). The specificity of reporter activity was determined by co-transfecting Cos7 cells with a DN-PPARγ expression vector. The presence of DN-PPARγ significantly reduced FM550-induced reporter expression (Figure 1A).

To examine the ability of FM550 to induce adipocyte differentiation, BMS2 cells were grown to confluence and then were treated with Vh or FM550. FM550 significantly induced lipid accumulation at concentrations ≥5 μg/ml (10 μM)(Figure 1B). The maximal FM550-induced lipid accumulation of 732±138 RFUs was less than the lipid accumulation induced by a maximally efficacious concentration of rosiglitazone (1 μM; 1043±45 RFUs; see Supplemental Material, Figure S2B). In order to confirm that FM550 stimulated terminal adipocyte differentiation, BMS2 cells were assessed for expression of the adipocyte-specific protein perilipin (Greenberg et al. 1991). Treatment with FM550 resulted in increased expression of

perilipin (Figure 1C). The results indicate that FM550 contains a component or components capable of activating PPARγ and stimulating adipocyte differentiation.

Computational and *in vitro* analyses of PPARγ binding by components of FM550

To test the hypothesis that components of FM550 are PPARγ ligands, we next assessed the ability of FM550 and its components to bind with the PPARγ LBD (Figure 2). We found that FM550 could competitively bind with the PPARγ LBD in a dose-dependent manner (IC_{50}: 400 μM; K_d = 210 μM). The brominated components of FM550, TBB and TBPH, did not demonstrate any binding over the concentration range tested. In contrast, TPP was found to be a ligand of PPARγ (IC_{50}: 38 μM; K_d 20 μM). ITP showed a similar ability to TPP to compete for PPARγ binding (IC_{50}: 60 μM; K_d: 32 μM). In comparison, rosiglitazone competed for PPARγ binding with an IC_{50} of 0.23 μM and K_d of 0.12 μM (see Supplemental Material, Figure S2C). Since ITP contains ~40% TPP (measured by H. Stapleton's laboratory), TPP was likely a significant contributor to PPARγ binding by the ITP mixture; however, the other isopropylated phosphate isomers in this mixture may also effectively bind to PPARγ-LBD.

Interaction of TPP and ITP with the PPARγ LBD was assessed computationally. Our earlier study using the FTMap solvent mapping program (Brenke et al. 2009) identified two main ligand binding regions within PPARγ's large binding site (Sheu et al. 2005). The first is located at the polar headgroup of thiazolidinediones (TZDs), interacting with the H12 helix of the LBD, and the second is between the distal end of TZDs and the entrance of the ligand binding site. Since the first region is too narrow for the binding of TPP, we focused on the second site, which is known to bind selective partial agonists (Bruning et al. 2007). Mapping of the latter region shows four binding hot spots (Figure 3A). As shown in Figure 3B, the locations of these hot spots are in good agreement with the positions of the three rings and the carboxylic acid group in

several selective partial agonists such as 5-chloro-1-(4-chlorobenzyl)-3-(phenylthio)-1h-indole-2-carboxylic acid (also called nTZDpa) that bind at this site and activate PPARγ using an H12 independent mechanism (Bruning et al. 2007). In the best docked mode of TPP, the three rings overlap with the three hot spots that also interact with the rings of nTZDpa (Figure 3C). Since ligands that bind to a site generally overlap well with binding hot spots (Hall et al. 2012), based on this results we are convinced that TPP binds to PPARγ in a manner very similar to the binding of selective partial agonists. We note that the hot spots extend beyond the rings, and thus PPARγ very likely also binds the various isopropylated derivatives of TPP (Figure 3D).

Assessment of PPARγ activation by the organophosphate components of FM550

As with FM550, we examined the ability of TPP and ITP to activate PPARγ-driven reporter expression and induce adipogenesis. In the PPARγ/RXRα Cos7 cell reporter assay, TPP significantly induced PPARγ-driven reporter activity at concentrations ≥10 μM, with an EC_{50} of 8 μM and maximal activity of 7.5±0.7-fold (Figure 4A), and ITP significantly induced PPARγ-driven reporter activity at concentrations ≥10 μg/ml (30 μM), with an EC_{50} of 8 μM and maximal activity of 5.1±0.6-fold (Figure 4A). TPP and ITP are less potent and efficacious than rosiglitazone (1 μM; 11.3±0.6-fold; EC_{50} of 0.02 μM; see Supplemental Material, Figure S2A). In the BMS2 adipogenesis assay, TPP significantly induced lipid accumulation at concentrations ≥5 μM with a maximal lipid accumulation of 614±60 RFUs (Figure 4B), and ITP significantly induced lipid accumulation at concentrations ≥1 μg/ml (3 μM), with a maximal lipid accumulation of 796±60 RFUs (Figure 4B). These were less than the lipid accumulation induced by a maximally efficacious concentration of rosiglitazone (1 μM; 1043±45 RFUs; see Supplemental Material, Figure S2B). That TPP and ITP induced terminal adipocyte differentiation was confirmed by the observation that both compounds induced the expression of

perilipin (Figure 4C). The results indicate that TPP and ITP are PPARγ ligands, which can induce adipocyte differentiation.

Analysis of effects of FM550 and TPP on bone differentiation *in vitro*

To test the hypothesis that FM550 and TPP are negative regulators of bone formation, we examined the effect of the FM550 and TPP on adipogenic and osteogenic differentiation in primary bone marrow cultures prepared from female C57BL/6J mice. Established bone marrow cultures were induced to undergo osteogenesis and treated with Vh, FM550, TPP or rosiglitazone. FM550 induced significant lipid accumulation at a concentration of 5 μg/ml (10 μM), and TPP induced lipid accumulation at a concentration of 10 μM (Figure 5A). Activation of PPARγ by FM550 and TPP was reflected in the significantly increased mRNA expression of *Fabp4*, a PPARγ-target gene (Tontonoz et al. 1994) (Figure 5B). While FM550 significantly suppressed both alkaline phosphatase activity and mineralization at 5 μg/ml (10 μM), TPP only significantly suppressed alkaline phosphatase activity (Figs. 5C and D). Suppression of the transcriptional program of Runx2, the master regulator of osteogenesis, by FM550 and TPP was indicated by the significant decrease in mRNA expression of *Sp7*, a Runx2-target gene (Bonewald 2011) (Figure 5E). Taken together, these results suggest that FM550 and TPP can divert MSC differentiation away from osteogenesis and towards adipogenesis and that the FM550 mixture, as a whole, may have a greater effect than TPP.

Estimated indoor exposure of children to TPP

We used a recently published screening-level exposure model for SVOCs (Little et al. 2012) to estimate the contribution of dust to TPP exposure. The geometric mean concentration of the log-normally distributed TPP in 50 Boston house dust samples was 7.36 μg/g (range <0.15-1800)

(Stapleton et al. 2009). Applying equations 2 and 3 (see Materials and Methods) to the geometric mean dust concentration estimated an indoor vapor concentration of 3.4 ng/m^3 (85% of total air concentration) and y_0 of 7.2 ng/m^3. Table 1 shows the estimated exposure to TPP by route for 3 year old children based on these indoor concentrations. Overall estimated exposure was 0.5 μg/day with 87% due to dust ingestion. Use of the maximum TPP dust concentration from Stapleton et al (2009), 1800 μg/g, yields an estimated total indoor exposure for children of 120 μg/day with the same breakdown by exposure pathway.

Discussion

Obesity and osteoporosis are two of the most pervasive chronic health care problems in the industrialized world. It has been proposed that exposure to environmental obesogens, chemicals that disrupt the homeostatic controls of adipogenesis and energy balance (Grun et al. 2006), is playing a role in the obesity epidemic. That a growing number of environmental PPARγ agonists are being shown to not only enhance adipocyte differentiation, but also suppress osteogenesis suggests that environmental toxicants may contribute to loss of bone health. A previous study showed that pre- and postnatal exposure to FM550 resulted in obesity, increased anxiety and early puberty in rats (Patisaul et al. 2013). Here, we show that the flame retardant mixture FM550 contains PPARγ ligands and stimulates adipogenesis, and we identify a novel PPARγ ligand, TPP, which modifies MSC differentiation.

FM550 binds to the human PPARγ LBD, activates human PPARγ1 transcriptional activity, and stimulates adipogenesis. PPARγ is the master regulator of adipocyte differentiation (Tontonoz and Spiegelman 2008), and its activation by thiazolidinedione drugs increases fat mass and weight gain (Carmona et al. 2005). Taken together, these results suggest that the increased fat

mass observed in rats treated perinatally with FM550 (Patisaul et al. 2013) results from PPARγ activation.

FM550 is a mixture of brominated components (TBB and TBPH) and triaryl phosphates (TPP and ITP). Previous analyses of the brominated components of FM550 showed that a brominated metabolite of TBPH, mono-(2-ethylhexyl) tetrabromophthalate, induced adipocyte differentiation in NIH 3T3L1 cells, and activated PPARα- and PPARγ-mediated gene transcription *in vitro* (Springer et al. 2012). However, TBPH is minimally metabolized into the monoester *in vivo* and *in vitro* (Patisaul et al. 2013; Roberts et al. 2012). Here we show that the brominated components of FM550 did not bind PPARγ. However, both TPP and ITP (which contains 40% TPP) bind to the human PPARγ LBD, interact with binding hot spots within the LBD, activate PPARγ1 transcriptional activity, and stimulate adipogenesis in a mouse bone marrow MSC model. Interestingly, the tri-substituted OPFRs have a structural similarity to organotins, a class of compounds for which the tri-substitution is known to be important for obesogenic activity (Grun et al. 2006). Thus, TPP is likely a significant contributor to the obesogenic activity of FM550.

Osteoporosis has been referred to as "obesity of the bone" (Rosen and Bouxsein 2006). PPARγ plays a crucial role in MSC differentiation, both by activating adipogenic differentiation and by suppressing osteoblast differentiation (Akune et al. 2004). Accordingly, treatment with the therapeutic PPARγ ligand, rosiglitazone, either *in vivo* or in *in vitro* bone marrow MSC models results in increased expression and activity of PPARγ and a concomitant decrease in Runx2 expression and activity (Ali et al. 2005; Rzonca et al. 2004). Here we show that FM550 and TPP can divert bone marrow MSC differentiation away from bone formation and toward adipocyte differentiation. These findings point to the need for serious consideration as to whether

environmental PPARγ ligands (e.g. TPP, phthalates and organotins) also have detrimental effects on bone health by accelerating osteoporosis or enhancing osteoporotic pathology.

The organophosphate components of FM550 had significant biological activity at concentrations of 1-10 μM. The number of assessments of human exposure to OPFRs is growing; however few studies of human body burden exist. Analyses of OPFRs in human milk showed that TPP is a common contaminant and that levels of total OPFRs can reach 600 ng/g lipid (Kim et al. 2014). For comparison, a molar concentration of OPFRs of 0.1 μM can be estimated by assuming a concentration of 41 g lipid/l milk (Kent et al. 2006) and an average OPFR molecular weight of 300 g/mol (the molecular weight of TPP is 326 g/mol).

Little information is available on indoor exposure of children to TPP, and the relative importance of dust ingestion for TPP is unknown. Most previous estimates of exposure to flame retardants such as PentaBDE suggest that dust ingestion is much more important to exposure than inhalation, particularly for children. However, the vapor pressure of TPP is 1-2 orders of magnitude higher than BDE-47 and BDE-99, major components of PentaBDE (Weschler and Nazaroff 2008). Furthermore, few estimates have been made of dermal absorption of flame retardants from vapor. Nevertheless, our modeling suggests that dust ingestion accounts for about 87% of exposure in 3-year old children with the remainder roughly split between inhalation and dermal absorption of vapor. Meeker et al (2013) recently reported no significant association between DPP in urine of adult males and TPP in dust from their homes. They listed several potential explanations, including logistics of the sample collections, exposure in other microenvironments and exposure via inhalation. Our modeling suggests that exposure to house dust is the major route of exposure for young children at home with inhalation and dermal absorption of TPP playing small but non-negligible roles. These estimates rely on a number of

assumptions, e.g., dust ingestion rates are relatively uncertain. Other exposure routes are not included, e.g., dermal absorption following contact with dust, surface films or personal care products (Little et al 2012). Hence, additional research on exposure to TPP is needed. Use of the maximum TPP dust concentration from the 50 Boston homes yielded an exposure estimate for children of 120 μg/day or approximately 9 μg/kg/day of TPP. For comparison, Patisaul exposed dams to 0.1 and 1 mg/day of FM550, or approximately 0.25-2.5 mg/kg/day, of which TPP represented approximately 10-20% (Patisaul et al. 2013). While there are several difficulties in making these comparisons, they suggest that additional, lower dose toxicological studies are needed to determine if current exposure to TPP and other PPARγ ligands pose health risks.

Conclusions

Results from this study support the conclusion that the alternative flame retardant mixture FM550 may be obesogenic because it contains a PPARγ ligand(s). The likely mediator of the adipogenic effect of FM550 is TPP, as TPP binds PPARγ, activates PPARγ-mediated transcription and induced adipogenesis. That FM550 and TPP are adipogenic has implications for both development of obesity and loss of bone health in humans.

References

Akune T, Ohba S, Kamekura S, Yamaguchi M, Chung UI, Kubota N, et al. 2004. PPARγ insufficiency enhances osteogenesis through osteoblast formation from bone marrow progenitors. J Clin Invest 113:846–855.

Ali AA, Weinstein RS, Stewart SA, Parfitt AM, Manolagas SC, Jilka RL. 2005. Rosiglitazone causes bone loss in mice by suppressing osteoblast differentiation and bone formation. Endocrinology 146:1226–1235.

ARChem. 2013. SPARC performs automated reasoning in chemistry. http://www.archemcalc.com/sparc.html. Accessed July 9, 2014.

BHFTI. 2000. Technical bulletin 117: Requirements, test procedure and apparatus for testing the flame retardance of resilient filling materials used in upholstered furniture. http://www.bhfti.ca.gov/industry/117.pdf.

Bonewald LF. 2011. The amazing osteocyte. J Bone Miner Res 26:229–238.

Bradford MM. 1976. A rapid and sensitive method for the quantitation of microgram quantities of protein utilizing the principle of protein-dye binding. Anal Biochem 72:248–254.

Brenke R, Kozakov D, Chuang GY, Beglov D, Hall D, Landon MR, et al. 2009. Fragment-based identification of druggable 'hot spots' of proteins using fourier domain correlation techniques. Bioinformatics 25:621–627.

Bruning JB, Chalmers MJ, Prasad S, Busby SA, Kamenecka TM, He Y, et al. 2007. Partial agonists activate ppargamma using a helix 12 independent mechanism. Structure 15:1258–1271.

Carignan CC, McClean MD, Cooper EM, Watkins DJ, Fraser AJ, Heiger-Bernays W, et al. 2013. Predictors of tris(1,3-dichloro-2-propyl) phosphate metabolite in the urine of office workers. Environ Int 55:56–61.

Carmona MC, Louche K, Nibbelink M, Prunet B, Bross A, Desbazeille M, et al. 2005. Fenofibrate prevents rosiglitazone-induced body weight gain in ob/ob mice. Int J Obesity 29:864–871.

Cooper EM, Covaci A, van Nuijs AL, Webster TF, Stapleton HM. 2011. Analysis of the flame retardant metabolites bis(1,3-dichloro-2-propyl) phosphate (BDCPP) and diphenyl phosphate (DPP) in urine using liquid chromatography-tandem mass spectrometry. Anal Bioanal Chem 401:2123–2132.

Dodson RE, Perovich LJ, Covaci A, Van den Eede N, Ionas AC, Dirtu AC, et al. 2012. After the PBDE phase-out: A broad suite of flame retardants in repeat house dust samples from California. Environ Sci Technol 46:13056–13066.

Feige JN, Gelman L, Rossi D, Zoete V, Metivier R, Tudor C, et al. 2007. The endocrine disruptor monoethyl-hexyl-phthalate is a selective peroxisome proliferator-activated receptor gamma modulator that promotes adipogenesis. J Biol Chem 282:19152–19166.

Feige JN, Gerber A, Casals-Casas C, Yang Q, Winkler C, Bedu E, et al. 2010. The pollutant diethylhexyl phthalate regulates hepatic energy metabolism via species-specific PPARα-dependent mechanisms. Environ Health Perspect 118:234–241.

Greenberg AS, Egan JJ, Wek SA, Garty NB, Blanchette-Mackie EJ, Londos C. 1991. Perilipin, a major hormonally regulated adipocyte-specific phosphoprotein associated with the periphery of lipid storage droplets. J Biol Chem 266:11341–11346.

Grun F, Watanabe H, Zamanian Z, Maeda L, Arima K, Cubacha R, et al. 2006. Endocrine-disrupting organotin compounds are potent inducers of adipogenesis in vertebrates. Mol Endocrinol 20:2141–2155.

Gurnell M, Wentworth JM, Agostini M, Adams M, Collingwood TN, Provenzano C, et al. 2000. A dominant-negative peroxisome proliferator-activated receptor gamma (PPARγ) mutant is a constitutive repressor and inhibits PPARγ-mediated adipogenesis. J Biol Chem 275:5754–5759.

Hall DR, Ngan CH, Zerbe BS, Kozakov D, Vajda S. 2012. Hot spot analysis for driving the development of hits into leads in fragment-based drug discovery. J Chem Inf Model 52:199–209.

Honkakoski P, Palvimo JJ, Penttila L, Vepsalainen J, Auriola S. 2004. Effects of triaryl phosphates on mouse and human nuclear receptors. Biochem Pharmacol 67:97–106.

Kent JC, Mitoulas LR, Cregan MD, Ramsay DT, Doherty DA, Hartmann PE. 2006. Volume and frequency of breastfeedings and fat content of breastmilk throughout the day. Pediatrics 11&:e378–395.

Kim JB, Wright HM, Wright M, Spiegelman BM. 1998. ADD1/SREBP1 activates PPARγ through the production of endogenous ligand. Proc Natl Acad Sci U S A 95:4333–4337.

Kim JW, Isobe T, Muto M, Tue NM, Katsura K, Malaryannan G, et al. 2014. Organophosphorus flame retardants (PFRs) in human breast milk from several Asian countries. Chemosphere

Kojima H, Takeuchi S, Itoh T, Iida M, Kobayashi S, Yoshida T. 2013. In vitro endocrine disruption potential of organophosphate flame retardants via human nuclear receptors. Toxicology 314:76–83.

Kozakov D, Hall DR, Chuang GY, Cencic R, Brenke R, Grove LE, et al. 2011. Structural conservation of druggable hot spots in protein-protein interfaces. Proc Natl Acad Sci U S A 108:13528–13533.

Little JC, Weschler CJ, Nazaroff WW, Liu Z, Cohen Hubal EA. 2012. Rapid methods to estimate potential exposure to semivolatile organic compounds in the indoor environment. Environ Sci Technol 46:11171–11178.

Meeker JD, Cooper EM, Stapleton HM, Hauser R. 2013. Urinary metabolites of organophosphate flame retardants: Temporal variability and correlations with house dust concentrations. Environ Health Perspect 121:580–585.

Patisaul HB, Roberts SC, Mabrey N, McCaffrey KA, Gear RB, Braun J, et al. 2013. Accumulation and endocrine disrupting effects of the flame retardant mixture Firemaster® 550 in rats: An exploratory assessment. J Biochem Mol Toxicol 27:124–136.

Pfaffl MW. 2001. A new mathematical model for relative quantification in real-time RT-PCR. Nucleic Acids Res 29:e45.

Pietrangeli C, Hayashi S-I, Kincade P. 1988. Stromal cell lines which support lymphocyte growth: Characterization, sensitivity to radiation and responsiveness to growth factors. Eur J Immunol 18:863–872.

Roberts SC, Macaulay LJ, Stapleton HM. 2012. In vitro metabolism of the brominated flame retardants 2-ethylhexyl-2,3,4,5-tetrabromobenzoate (TBB) and bis(2-ethylhexyl) 2,3,4,5-tetrabromophthalate (TBPH) in human and rat tissues. Chem Res Toxicol 25:1435–1441.

Rosen CJ, Bouxsein ML. 2006. Mechanisms of disease: Is osteoporosis the obesity of bone? Nat Clin Pract Rheumatol 2:35–43.

Rzonca SO, Suva LJ, Gaddy D, Montague DC, Lecka-Czernik B. 2004. Bone is a target for the antidiabetic compound rosiglitazone. Endocrinology 145:401–406.

Sheu SH, Kaya T, Waxman DJ, Vajda S. 2005. Exploring the binding site structure of the PPARγ ligand-binding domain by computational solvent mapping. Biochemistry 44:1193–1209.

Springer C, Dere E, Hall SJ, McDonnell EV, Roberts SC, Butt CM, et al. 2012. Rodent thyroid, liver, and fetal testis toxicity of the monoester metabolite of bis-(2-ethylhexyl) tetrabromophthalate (TBPH), a novel brominated flame retardant present in indoor dust. Environ Health Perspect 120:1711–1719.

Stapleton HM, Allen JG, Kelly SM, Konstantinov A, Klosterhaus S, Watkins D, et al. 2008. Alternate and new brominated flame retardants detected in U.S. house dust. Environ Sci Technol 42:6910–6916.

Stapleton HM, Klosterhaus S, Eagle S, Fuh J, Meeker JD, Blum A, et al. 2009. Detection of organophosphate flame retardants in furniture foam and U.S. house dust. Environ Sci Technol 43:7490–7495.

Stapleton HM, Sharma S, Getzinger G, Ferguson PL, Gabriel M, Webster TF, et al. 2012. Novel and high volume use flame retardants in us couches reflective of the 2005 pentaBDE phase out. Environ Sci Technol 46:13432–13439.

Suzuki G, Tue NM, Malarvannan G, Sudaryanto A, Takahashi S, Tanabe S, et al. 2013. Similarities in the endocrine-disrupting potencies of indoor dust and flame retardants by using human osteosarcoma (U2OS) cell-based reporter gene assays. Environ Sci Technol 47:2898–2908.

Tontonoz P, Hu. E, Graves RA, Budavari AI, Spiegelman BM. 1994. mPPAR gamma 2: Tissue-specific regulator of an adipocyte enhancer. Genes Dev 8:1224–1234.

Tontonoz P, Spiegelman BM. 2008. Fat and beyond: The diverse biology of PPARgamma. Annu Rev Biochem 77:289–312.

Trott O, Olson AJ. 2010. AutoDock Vina: Improving the speed and accuracy of docking with a new scoring function, efficient optimization, and multithreading. J Comput Chem 31:455–461.

Van den Eede N, Dirtu AC, Neels H, Covaci A. 2011. Analytical developments and preliminary assessment of human exposure to organophosphate flame retardants from indoor dust. Environ Int 37:454–461.

Weschler CJ, Nazaroff WW. 2008. Semivolatile organic compounds in indoor environments. Atmos Environ 42:9018−9040.

Yanik SC, Baker AH, Mann KK, Schlezinger JJ. 2011. Organotins are potent activators of PPARγ and adipocyte differentiation in bone marrow multipotent mesenchymal stromal cells. Toxicol Sci 122:476–488.

Table 1. Estimated exposure of 3-year old children to TPP (based on geometric mean dust concentrations from 50 Boston homes).

Exposure pathway	Exposure (µg/day)	% of total
Inhalation (vapor)	0.028	5.5%
Inhalation (particles)	0.005	0.9%
Ingestion (dust)	0.44	87%
Dermal sorption (from vapor)	0.031	6.1%
Total	0.50	100%

Assumes: inhalation rate of 8.9 m^3/d, dust ingestion rate of 60 mg/d, exposed skin surface area of 0.61 m^2, exposure duration of 21.9 hr/d (Little et al. 2012).

Figure legends

Figure 1. Reporter and *in vitro* differentiation analyses of PPARγ activation by FM550. (A) Cos-7 cells were transiently transfected with human *PPARG1* and PPRE x3-TK-luc, with either pcDNA3 or PPARγ-DN vectors. Transfected cultures were treated with Vh (DMSO, reported as 10^{-2} μM) or FM550 (0.1-20 μg/ml; 0.2-50 μM) and incubated for 24 hrs. Reporter activation was assessed by luciferase expression and normalized by eGFP fluorescence. (B-C) Confluent BMS2 cultures were treated with Vh (DMSO, reported as 10^{-2} μM) or FM550 (0.1-10 μg/ml; 0.2-20 μM). Lipid accumulation (B) and perilipin expression (C) were quantified after 7 days. Data are representative of or are presented as means ± SE from 3-7 biological replicates. Statistically different from Vh-treated (*$p<0.05$, **$p<0.01$, ANOVA, Dunnett's).

Figure 2. Determination of PPARγ ligand binding affinities of FM550 and its components. The PolarScreen™ PPARγ-competitor assay was used to determine binding affinities. FM550 (0.01-70 μg/ml; 0.02-160 μM), TPP (0.01-1400 μM), TBB (0.009-90 μM), TBPH (0.12-1200 μM), and ITP (0.01-28 μg/ml; 0.02-80 μM) were applied to the assay in DMSO. IC_{50}'s and dissociation constants were calculated as described in the Methods. Data are presented as means ± SE from 3 technical replicates. Data are representative of two independent experiments. Statistically different from lowest concentration (**$p<0.01$, ANOVA, Dunnett's).

Figure 3. Computational analysis of TPP and ITP interactions with the PPARγ LBD. (A) Mapping of the PPARγ LBD structure (PDB ID 2q5s). The protein is shown as grey cartoon, and representatives of probe clusters within the various consensus clusters are shown as lines. The color codes are as follows: CC1 (27 probe clusters) cyan, CC2 (17 probe clusters) magenta, CC3 (16 probe clusters) yellow, CC4 (13 probe clusters) salmon, and CC5 (9 probe clusters) blue. To

see the probe clusters some parts of the PPARγ were removed. (B) Close-up of the mapping results. The bound pose of the partial agonist nTZDpa (shown as green sticks) is superimposed for reference. As shown, the three rings of nTZDpa bind at the hot spots defined by the consensus clusters CC1, CC4, and CC5, respectively, whereas the carboxylic acid of nTZDpa orients toward CC2. (C) Best docked pose of TPP (shown as magenta sticks). The rings in TPP interact with the same three hot spots at CC1, CC4, and CC5. (D) Best docked poses for two isopropylated derivatives of TPP.

Figure 4. Reporter and *in vitro* differentiation analyses of PPARγ activation by TPP and ITP. (A) PPARγ reporter transfections were carried out as described in Figure 1A. Transfected cultures were treated with Vh (DMSO, reported as 10^{-2} μM), TPP (0.1-40 μM) or ITP (0.1-10 μg/ml; 0.3-60 μM) and incubated for 24 hrs. Reporter activation was assessed by luciferase expression and normalized by eGFP fluorescence. (B-C) Confluent BMS2 cultures were treated with Vh (DMSO, reported as 10^{-2} μM), TPP (0.1-20 μM), or ITP (0.1-10 μg/ml; 0.3-30 μM). Lipid accumulation (B) and perilipin expression (C) were quantified after 7 days. Data are representative of or are presented as means ± SE from 3-7 biological replicates. Statistically different from Vh-treated (*$p<0.05$, **$p<0.01$, ANOVA, Dunnett's).

Figure 5. Assessment of effects of FM550 and TPP on osteogenesis *in vitro*. Primary bone marrow cultures were established, and osteogenesis was initiated with the addition of ascorbate, β-glycerol phosphate, insulin and dexamethasone, except for Naïve wells. Cells were treated with Vh (DMSO), FM550 (0.1-10 μg/ml; 0.2-20 μM), TPP (0.1-10 μM) or rosiglitazone (0.1 μM) and cultured for 7 (gene expression) or 12 (phenotype) days. (A) Lipid accumulation. (B) *Fabp4* mRNA expression. (C) Alkaline phosphatase activity. (D) Mineralization. (E) *Sp7* mRNA

expression. Data are presented as means ± SE from 4-6 independent bone marrow preparations. Statistically different from Vh-treated (*$p<0.05$, **$p<0.01$, ANOVA, Dunnett's).

Figure 1

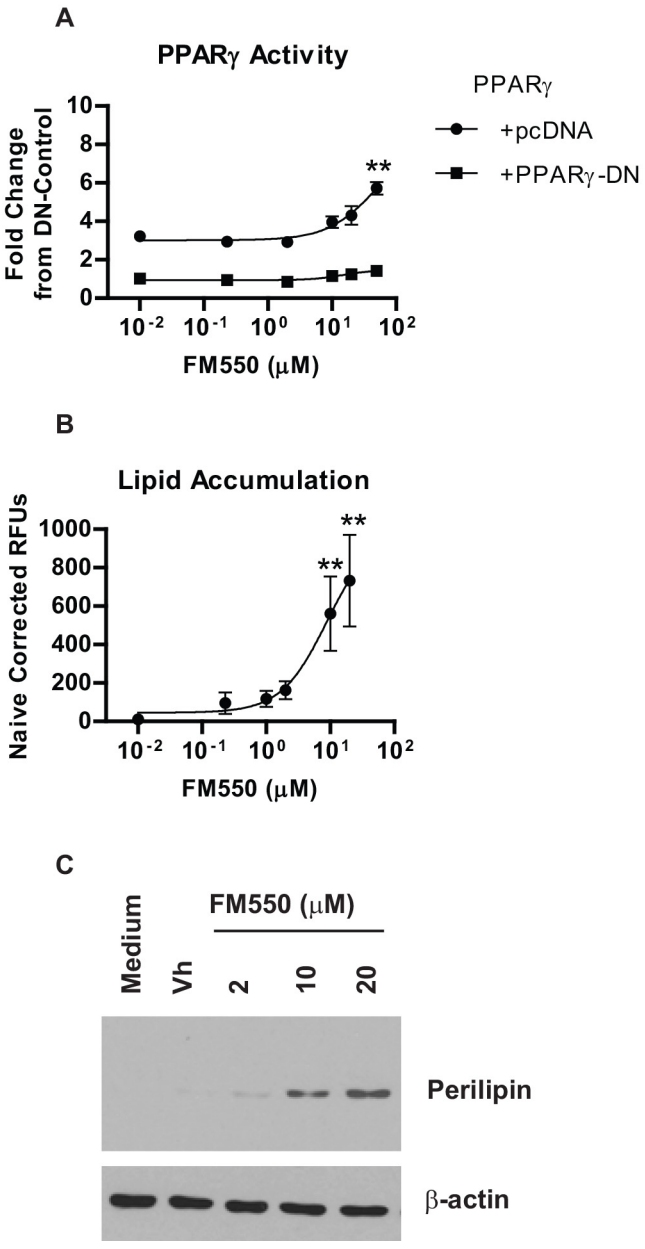
A
PPARγ Activity
PPARγ
+pcDNA
+PPARγ-DN
Fold Change from DN-Control
10
8
6
4
2
0
**
10-2 10-1 100 101 102
FM550 (μM)
B
Lipid Accumulation
Naive Corrected RFUs
1000
800
600
400
200
0
**
**
10-2 10-1 100 101 102
FM550 (μM)
C
Medium
Vh
FM550 (μM)
2
10
20
Perilipin
β-actin

Figure 2

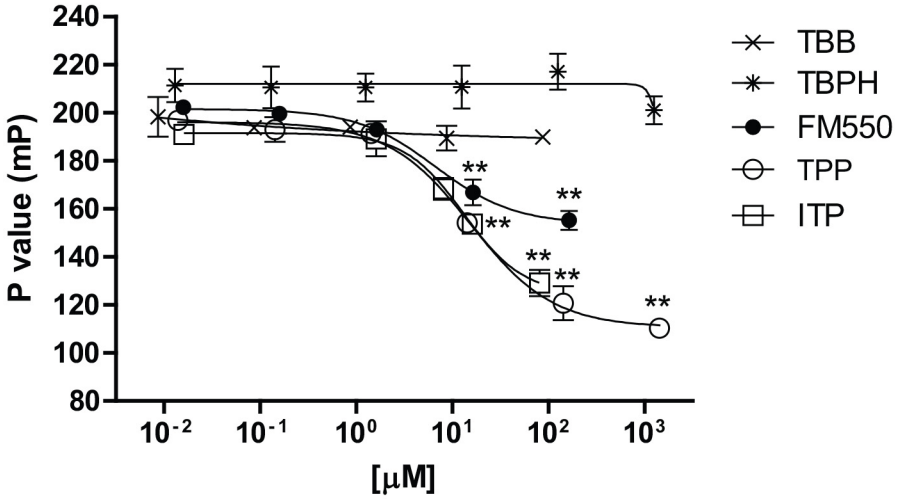
240
220
200
180
160
140
120
100
80
P value (mP)
10-2
10-1
100
101
102
103
[μM]
**
TBB
TBPH
FM550
TPP
ITP

Figure 3

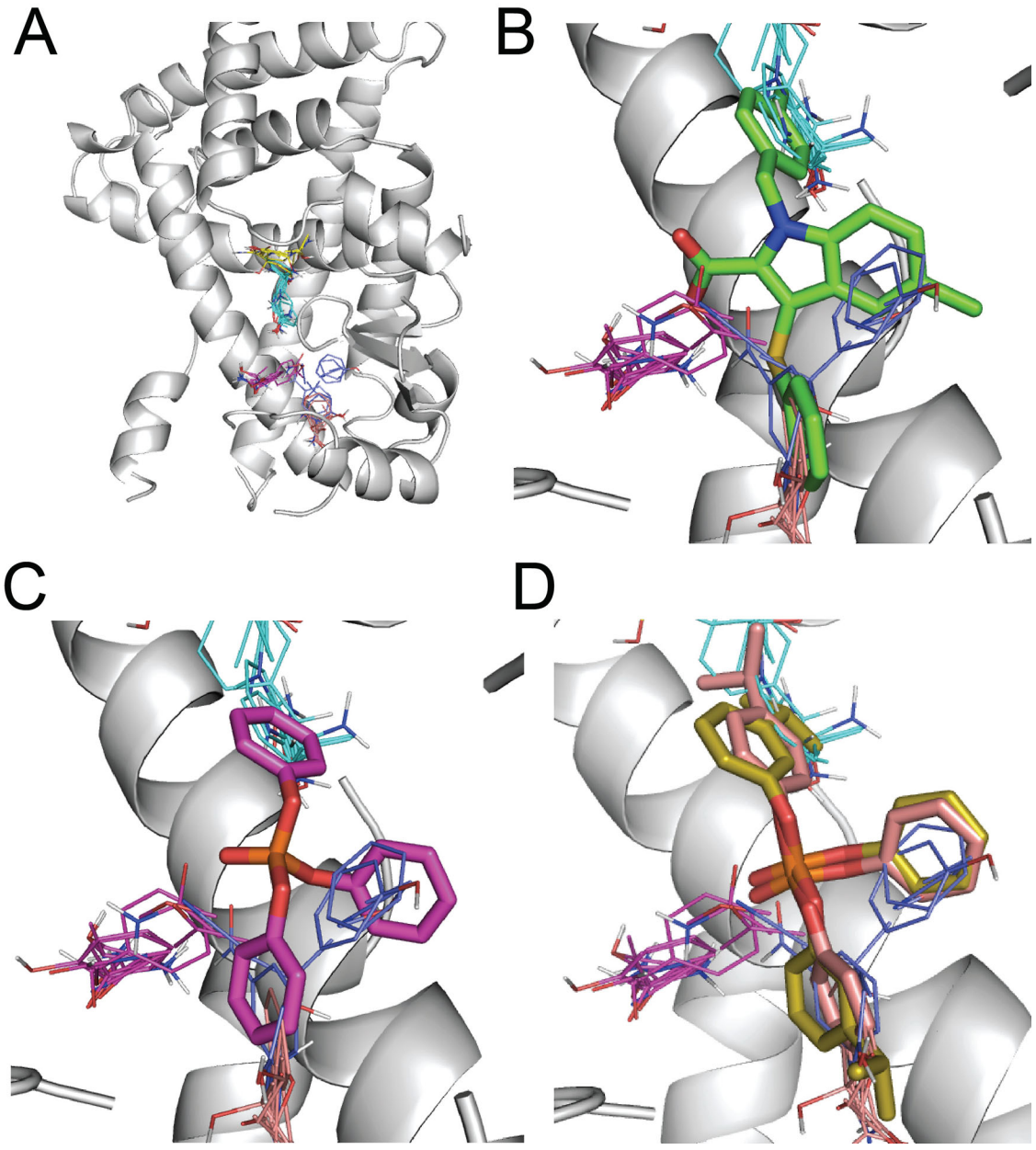

Figure 4

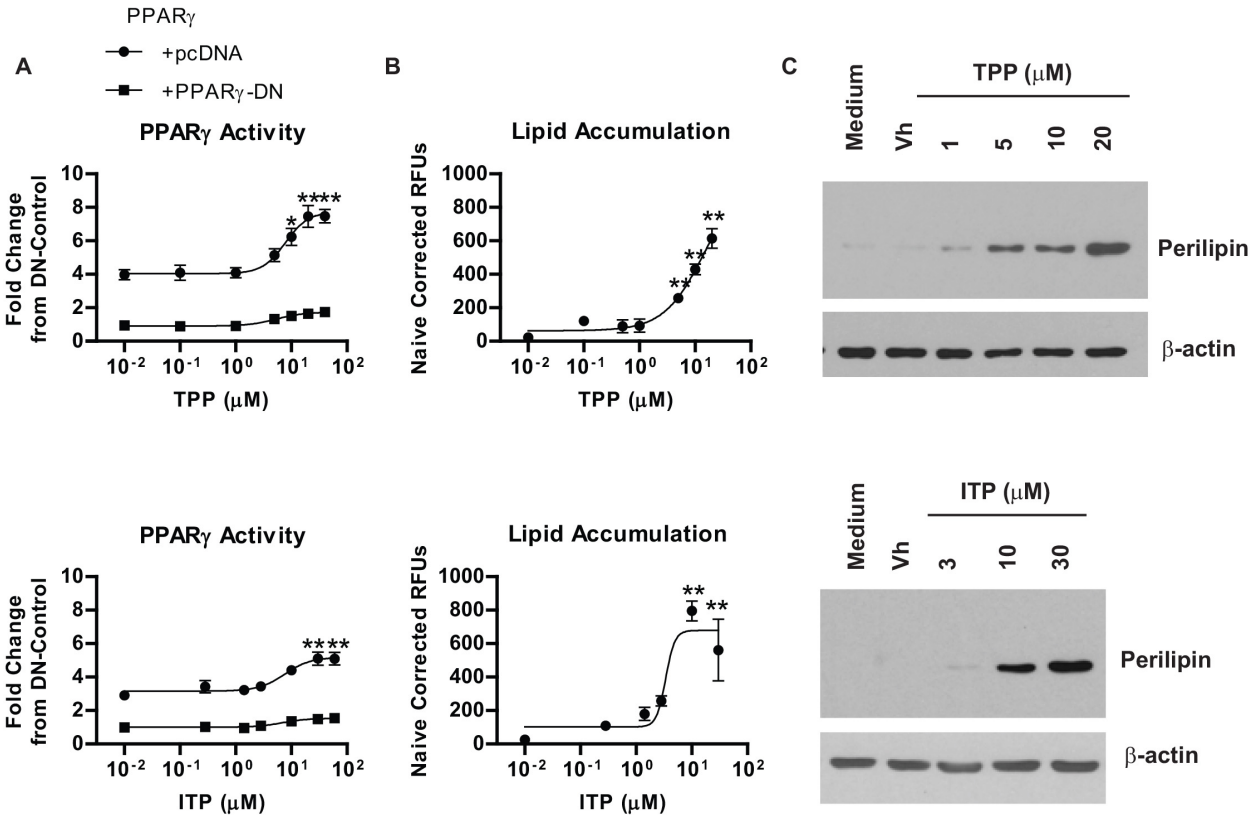
A
PPARγ
+pcDNA
+PPARγ-DN
PPARγ Activity
Fold Change from DN-Control
TPP (μM)
B
Lipid Accumulation
Naive Corrected RFUs
TPP (μM)
C
Medium
Vh
TPP (μM)
1
5
10
20
Perilipin
β-actin
PPARγ Activity
Fold Change from DN-Control
ITP (μM)
Lipid Accumulation
Naive Corrected RFUs
ITP (μM)
Medium
Vh
ITP (μM)
3
10
30
Perilipin
β-actin

Figure 5

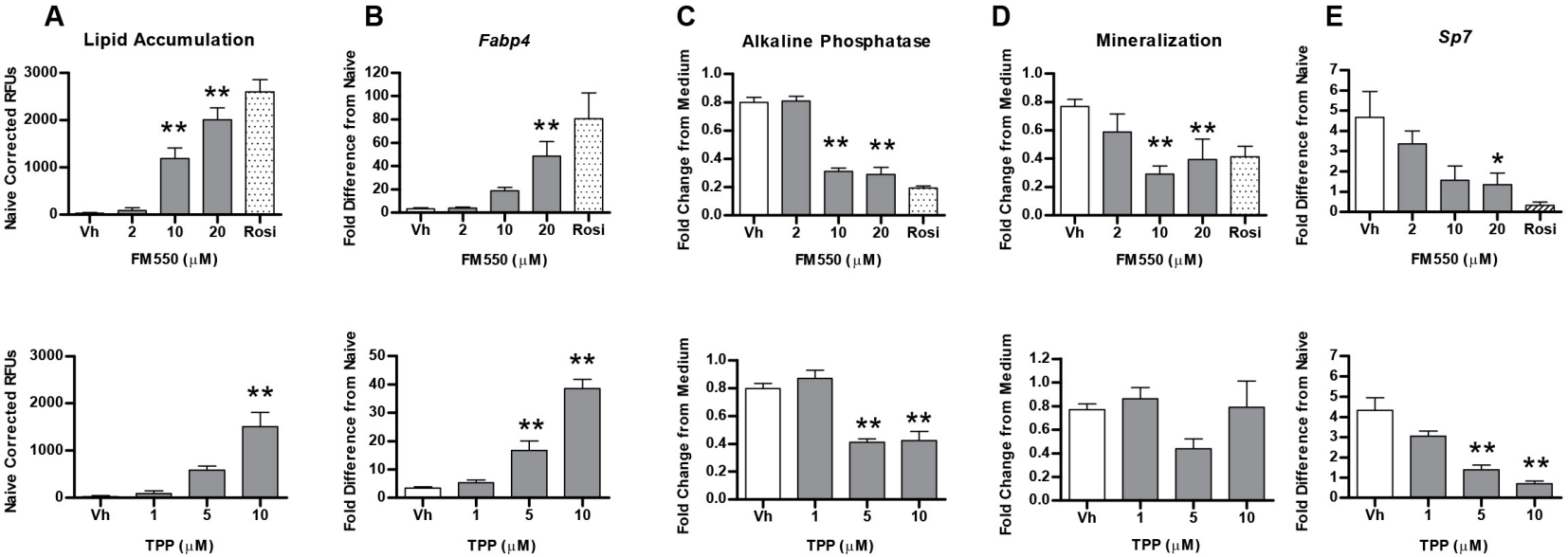
A
Lipid Accumulation
Naive Corrected RFUs
FM550 (μM)
Vh
2
10
20
Rosi
TPP (μM)
1
5
B
Fabp4
Fold Difference from Naive
C
Alkaline Phosphatase
Fold Change from Medium
D
Mineralization
E
Sp7